Food Structure 21 (2019) 100120

Contents lists available at ScienceDirect

Food Structure

journal homepage: www.elsevier.com/locate/foostr

Small and ultra-small angle neutron scattering studies of commercial milk

Carl P. Adams[a,*], Nukhalu Callaghan-Patrachar[a,b], Fernanda Peyronel[b], John Barker[c], David A. Pink[a,b], Alejandro G. Marangoni[b,*]

[a] Department of Physics, St. Francis Xavier University, Antigonish, NS B2G 2W5, Canada
[b] Biophysics Interdepartmental Group, University of Guelph, Guelph, ON N1G 2W1, Canada
[c] NIST Center for Neutron Research, National Institute of Standards and Technology, Gaithersburg, MD 20899, USA

ARTICLE INFO

Keywords:
Milk
Casein micelles
Schulz model
Neutron scattering

ABSTRACT

Milk and milk products are an essential part of global nutrition and the world-wide food industry. Studies of milk components using scattering techniques are well documented in the literature. However, those studies focused on the q scattering wavevector region $10^{-3} < q < 2\,\text{Å}^{-1}$. This manuscript presents scattering results in the region $3 \times 10^{-5} < q < 2 \times 10^{-2}\,\text{Å}^{-1}$, a region that allows the simultaneous study of fat globules and proteins found in commercial food-grade milk. The small and ultra-small angle neutron scattering (SANS and USANS) measurements show that a model based on the Schulz distribution function using uniform spheres was a reasonable choice to successfully fit the scattering features below $q = 0.007\,\text{Å}^{-1}$. Contrast measurements using D_2O on whole milk were carried out to distinguish fat from protein signals. Casein micelles were found to have mean diameters of 96 ± 10 nm with 33% polydispersity. The average scattering length density of the micelles varied from $-0.04 \times 10^{-6}\,\text{Å}^{-2}$ in homogenized, pasteurized commercial milk to $2.8 \times 10^{-6}\,\text{Å}^{-2}$ with 50% dilution by D_2O, with a match point of 43 ± 3%, as seen in previous studies. It was found that the average diameter of fat globules in homogenized whole milk was 0.47 ± 0.04 μm with a polydispersity of 45 ± 5%, and a volume fraction of 0.034 ± 0.002 when the scattering length density is fixed at $0.20 \times 10^{-6}\,\text{Å}^{-2}$. These USANS measurements provide an important foundation as similar techniques are employed to study cheese varieties and cheese formation.

1. Introduction

Milk is one of the most basic and oldest foods. Global milk production was estimated at 650 million tonnes in 2013 (ReportBuyer, 2014) and the annual value of the worldwide dairy industry is over 400 billion USD. In addition to its commercial importance, milk is interesting since its components appear at several different length scales in its native form and an even wider scale upon aggregation. Carbohydrates and whey proteins are the principle components in the serum phase of milk. The other principle components are found in a colloidal state. Casein proteins, along with calcium phosphate, aggregate to form hydrated micelles (Dalgleish & Corredig, 2012) while lipids are present inside globules (Goff, 2019) encased by membranes (Lopez, Madec, & Jimenz-Flores, 2010) that are modified after homogenization. These phases provide the majority of the protein and food energy available in milk and are key components in other dairy products, such as cheese. Hair-like molecular strands of κ-casein protrude from the surface to stabilize casein micelles (CMs) against aggregation in milk (de Kruif, 1999; Horne, 2006). Cheese is produced when the enzyme chymosin is introduced, the κ-casein protrusions are hydrolyzed, and CM aggregation takes place. The CMs and cheese formation have been studied with high-resolution transmission microscopy (McMahon & Oommen, 2008), cryo-scanning tunnelling microscopy (Ong, Dagastine, Kentish, & Gras, 2011), laser confocal microscopy (Ong, Dagastine, Kentish, & Gras, 2010; Ong et al., 2011) and dynamic light scattering (Gebhardt, Doster, Friedrich, & Kulozik, 2006). A less used but well-established technique in the study of food systems (Lopez-Rubio & Gilbert, 2009) is small-angle neutron scattering (SANS). SANS offers several advantages over techniques based on electromagnetic scattering. Neutrons can penetrate where visible light cannot. SANS can probe a wide range of length scales and has the advantage of being non-invasive and non-destructive. Sample preparation is reduced to a minimum when compared with the manipulation required for microscopy. The use of deuterium contrast matching is a highlight of this technique as it allows for the study of specific components without any chemical modification of the sample. This technique, along with small angle X-ray scattering (SAXS), has been frequently used to study the hierarchical structures at length scales between microns and nanometers that are found in milk and

* Corresponding authors.
E-mail addresses: cadams@stfx.ca (C.P. Adams), amarango@uoguelph.ca (A.G. Marangoni).

https://doi.org/10.1016/j.foostr.2019.100120
Received 20 February 2019; Received in revised form 23 June 2019; Accepted 28 June 2019
Available online 02 July 2019

dairy products (Kuo, Ilavsky, & Lee, 2016; Li et al., 2018; Tromp & Bouwman, 2007 and a review by de Kruif, 2014). Earlier work using SANS focused on understanding the internal structure of casein micelles (Alexander, Nieh, Ferrer, & Corredig, 2011; Hansen et al., 1996; Stothart, 1989; Stothart & Cebula, 1982). In an effort to concentrate on the CMs and micelle substructure, many groups have carried out scattering studies on systems where the CMs have been removed from milk and then re-introduced into milk serum (de Kruif, 2014; de Kruif, Huppertz, Urban, & Petukhov, 2012) or using skim milk powder (Jackson & McGillivray, 2011; van Heijkamp et al., 2010). Those researchers agreed that the CMs are polydisperse and independent, with a typical value for R_g (the radius of gyration) of 110 nm (de Kruif, 2014). The typical experimental scattering wavevector q range for these studies ran from 10^{-3} to 1 $Å^{-1}$. This is ideal for looking at the details of the CMs: the distribution of calcium and phosphorus, non-uniformity of micelle sub-structure and the smoothness of the micelle surface. There have also been studies conducted at lower q values. Previous X-ray scattering studies on CMs in milk serum have reached a minimum $q = 2 \times 10^{-4}$ $Å^{-1}$ (de Kruif, 2014) and recent measurements on an anhydrous fat-whey protein gel have reached $q = 1 \times 10^{-4}$ $Å^{-1}$ (Kuo et al., 2016). Published USANS measurements have been made to q values of 2×10^{-4} $Å^{-1}$ using multiple-crystal bounce Bonse–Hart type USANS instruments (Bonse & Hart, 1965; Jackson & McGillivray, 2011; Li et al., 2018) and to $q = 1 \times 10^{-5}$ $Å^{-1}$ using the double-crystal diffractometer USANS V12a at the Hans-Meitner Institute (van Heijkamp et al., 2010). Another technique employed to study independent and aggregated CMs is to use spin echo small angle neutron scattering (SESANS) (Tromp & Bouwman, 2007). These low-q measurements, when carried out on fat-free, uncoagulated samples, were in agreement with the previous findings about CMs size and showed no evidence for any length scale larger than the CMs.

The literature, however, lacks information regarding the simultaneous study of FM and CM from a commercial milk sample using scattering techniques. The fat globules (FGs) have been extensively studied using optical microscopy (Lopez, Cauty, & Guyomarc'h, 2015; Lopez et al., 2010) due to their larger sizes compared with CM. Lately, new insight (Goff, 2019) has been gained regarding the structural changes experienced by FGs and their membranes due to homogenization.

The goal of this work is to use scattering measurements to elucidate the sizes and morphology of the FGs and CMs in commercial milk. Some concerns have been raised about the effects of reconstitution on caseins from micellular casein isolate (de Kruif, 2014). Thus, in this research, measurements have been taken on commercial food grade milk without using milk powder, an ultra-centrifuge, or a serum of reconstituted casein protein.

This study uses a combination of SANS and USANS measurements with D_2O contrast variation up to 50%. SANS and the upper end of the USANS q-range was used to identify CM, while the lower end of the USANS ranges was used to study FGs. The combination of contrast variation, and a very broad q-range, allows for the use of a bimodal model to distinguish the signals from FGs and CMs, even though there is significant overlap of q and scattering intensity. This work in this extended q range will provide the foundation needed to understand the structures formed when studying cheeses and milk component aggregation, where light scattering and microscopy suffer limitations due to opacity.

2. Materials and methods

2.1. Neutron scattering

2.1.1. Basics of coherent neutron scattering

Using neutrons to study soft-condensed matter systems of biological interest is a mature subject and there are several excellent references for the technique (Grillo, 2008; Hammouda, 2010; Roe, 2000). At the most basic level, elastic scattering techniques involve an approximate plane wave neutron beam that is incident on the sample and the count rate dN/dt is measured at different scattering angles. The isotropic scattering is measured as a function of q, the magnitude of the change in wavevector. This manuscript uses units of reciprocal Ångstroms where $1\ Å^{-1} = 10\ nm^{-1}$. As a rough guide, $2\pi/q$ corresponds to the length scale that is being probed. The actual sample dependent quantity of interest is the scattering intensity $I(q)$, which is proportional to the count rate but removes the sample independent factors (the incident neutron flux, the solid angle of the detector and detector efficiency) and the sample dependent factors (sample transmission and volume). In this manuscript $I(q)$ is in units of $cm^{-1}\,sr^{-1}$ and represents differential cross-section (area per steradian) per unit volume of sample.

The strength of scattering from the sample is described by the coherent scattering length density, SLD or $\rho(\vec{r})$, which describes the density, strength, and effective scattered-wave phase shift due to the neutron scattering centres. The scattering length density can be calculated by adding the individual coherent scattering lengths (Sears, 1992) of each nucleus in a specified volume element and then dividing by the volume of that element. Coherent scattering at a non-zero q arises when there are spatial variations of $\rho(\vec{r})$ in the sample, for example, between colloidal particles with one value of ρ and a medium with a different value of ρ. Scattering depends on the square of the difference in ρ, thus, a very common technique in neutron scattering is contrast matching or contrast variation. The SLD of a water-based medium is controlled by using different combinations of H_2O and D_2O. Pure H_2O has $\rho = -0.5617 \times 10^{-6}$ $Å^{-2}$ and pure D_2O has $\rho = 6.405 \times 10^{-6}$ $Å^{-2}$ and the SLD of a solution comes from the volume-weighted average. Changing the medium SLD allows the masking ($\Delta\rho = 0$) or enhancement (increased $|\Delta\rho|$) of signals from different sample components in a non-invasive way.

2.1.2. The scattering model

The model chosen to describe the data includes two independent, dilute populations of uniform, smooth and non-interacting polydisperse spheres. Each distribution, $f(r)$, of radius r is given by the normalized Schulz distribution (Kotlarchyk & Chen, 1983).

$$f(r) = (z+1)^{z+1}\left(\frac{r}{R_{avg}}\right)^{z}\frac{\exp[-(z+1)r/R_{avg}]}{R_{avg}\Gamma(z+1)} \quad (1)$$

Here, Γ is the gamma function, R_{avg} is the mean radius and z is related to the polydispersity. If σ^2 is the variance of the distribution and the polydispersity is $p = \sigma/R_{avg}$, then the parameter $z = 1/p^2 - 1$. Because of the two populations this model is usually called the bimodal Schulz distribution. The key parameters of this model are the SLD of the medium (the independent variable when doing contrast variation), background, and then volume fractions, SLDs, diameter-weighted average diameters, and polydispersities for the two populations. In whole milk, one group of spheres could be used to describe the CMs and the other group, the FGs. In this model it is assumed that each sphere is independent of all of the others in either population so there is no structure factor. The model also assumes that there is no internal structure to either CMs or FGs, nor is there any special structure of the outer layers. This assumption certainly fails when probing higher values of q but the model is remarkably effective otherwise. There was no *a priori* reason to choose the Schulz distribution over, for example, a log-normal distribution, but it is a common choice that allows for a significant reduction in calculation time because several integrals can be handled analytically. This choice does not make any significant difference to the result for modest levels of polydispersity where the differences in peak shape between the distributions are small.

2.1.3. Invariant calculations

It is also possible to obtain important, model-independent information from $I(q)$. With a uniform medium and a single scattering

phase (SP) in suspension there is a simple relation between an integral of $I(q)$ called the invariant Γ_0 (or Q in some references), the volume fraction ϕ of the SP and $\Delta\rho$, the difference in SLD between the medium and the SP.

$$\Gamma_0 = \int_0^\infty q^2 I(q) \mathrm{d}q = 2\pi^2(\Delta\rho)^2\phi \tag{2}$$

Assuming the entire $I(q)$ curve is measured, this relationship is true for any structure or polydispersity of the SP; so, in that sense, it is model independent. There is some uncertainty since it is not possible to experimentally measure $I(q)$ over an infinite range. To account for these unknown regions a Guinier model [$I(q) \propto \exp(-kq^2)$, k is a constant related to R_g] is used to extrapolate to low q and a Porod model [$I(q) \propto q^{-4}$] is used to extend to high q (Roe, 2000).

The invariant equation can be rearranged to give information about $\Delta\rho$.

$$\rho_{SP} - \rho_{medium} = \pm \frac{1}{\sqrt{2}\pi\phi^{1/2}} \Gamma_0^{1/2} \tag{3}$$

Usually these measurements are made while changing the value of ρ_{medium} with contrast variation, so it is appropriate to use a positive sign on one side of the match point ($\Delta\rho = 0$) and the negative sign on the other.

2.1.4. Smearing effects in USANS measurements

Resolution is a further important consideration when comparing a calculated $I(q)$ to the scattering intensity from the instrument. This was discussed by Pederson (1993). For Bonse–Hart geometry instruments (Bonse & Hart, 1965), like the BT5 USANS instrument at the NIST Centre for Neutron Research (NCNR) (Barker et al., 2005), the extremely high q resolution in one direction comes from the perfect crystal monochromator and analyzer. At the same time, resolution is sacrificed in the orthogonal direction (Δq_z) to increase the intensity. The same effect is seen in X-ray instruments that use the Bonse–Hart geometry (Ilavsky et al., 2009). The data measured is "smeared" compared to a pinhole geometry; there is a fairly wide range of q included in each measured point of nominal q. The actual value for q varies between the nominal q, as indicated by scattering angle, up to a value of $\sqrt{q_{nom}^2 + \Delta q_z^2}$. Assuming that the scattering angle is changing in the horizontal plane as the analyzer rotates, then $\pm \Delta q_z$ represents the vertical or orthogonal window accepted by the spectrometer. Therefore, the smeared intensity $I_s(q)$ from USANS represents an average (Kline, 2006).

$$I_s(q) = \frac{1}{2\Delta q_z} \int_{-\Delta q_z}^{\Delta q_z} I\left(\sqrt{q^2 + q_z^2}\right) dq_z = \frac{1}{\Delta q_z} \int_0^{\Delta q_z} I\left(\sqrt{q^2 + q_z^2}\right) dq_z \tag{4}$$

At first it might appear that a Δq_z that is much larger than the nominal q would cause so much systematic error that the data would be useless,[1] but for many forms of $I(q)$ this is not the case. For example, if $I(q)$ can be characterized by a power law in a q region with exponent $-p$ and $p > 1$, then $I_s(q)$ will also be a power law with an exponent of $-(p-1)$.

One way to deal with smearing is to use the analysis program to calculate a trial $I(q)$ that matches the measured $I_s(q)$ (the data is "desmeared"). There is a certain ambiguity with this method since the $I(q)$ is not necessarily unique and extra uncertainties may be introduced when choosing an extrapolation to higher q for the integral in Eq. (4), but it does allow for a plot of $I(q)$ without a model. The extrapolation means that the potential error associated with this method grows if $I_s(q)$ is known in only a limited q range, which is the case for USANS measurements. Noisy data from small signals can also lead to extra uncertainties when it is processed to obtain an $I(q)$ from $I_s(q)$. This is the case for the USANS signal from CMs alone at the volume fraction and contrast in commercial milk. The alternative method is to leave the USANS data as $I_s(q)$, select a scattering model $I(q)$ with adjustable parameters, and then use Eq. (4) to produce $I_s(q)$. There is no uncertainty when transforming in this manner since an $I(q)$ produces a unique $I_s(q)$. The $I_s(q)$ is compared to the measured data and the parameters in the model are adjusted accordingly. In addition to different slopes, $I(q)$ and $I_s(q)$ have different vertical scales. All of the model parameters (average diameter, polydispersity etc.) given in the text and tables are appropriate for $I(q)$ but some data and models are presented in figures as $I_s(q)$ (i.e. as it would be recorded by a USANS instrument). Note that if $I(q)$ has a slope of zero approaching $q = 0$, then $I_s(q)$ also has a slope of zero approaching $q = 0$, but with a different asymptotic value for scattered intensity.

2.1.5. Analysis and quoted uncertainties

The data analysis and reduction was primarily carried out with the *Igor Pro* program along with the analysis macros provided by the NCNR staff (Kline, 2006). The bimodal Schulz model, conversion to absolute units, calculation of invariant, and smearing/desmearing procedures are included with these macros. The routines also give a comparison between the wide angle and peak transmission to give an indication of multiple scattering. This was not a problem for the samples used here and their thicknesses.

Throughout this manuscript, uncertainties are quoted for measured quantities that arise from fitting models to data, rather than direct measurements. The general guideline used is to estimate these uncertainties such that there is 90% confidence that the true value lies within the quoted uncertainty range. Because results are based on fits to data, often with coupled parameters, this estimate is based on a combination of acceptable fit quality and physically reasonable parameters (i.e., establishing a range over which the fitting parameters provide a reasonable description of the data using the chosen physical model). If calculating fit quality as a reduced χ_ν^2, then the fit becomes unreasonable when χ_ν^2 increases by 10% or 20% from its minimum value. At this point there is usually a clear visual deterioration in the fit quality. This graphical disagreement can be harder to judge with global fits, when for example, each individual scattering curve does not have its own effective scaling. In this circumstance, a global fit yields $I(q)$ of some models above individual $I(q)$ curves and others below. It is also impractical, even when using a global fitting procedure, to allow the free variation of all parameters involved. If parameters are clearly and strongly coupled (such as volume fraction and SLD difference) independent measurements or information is used to fix parameters (e.g., volume fraction of CMs in milk, SLD of milk serum as a function of D_2O content, SLD of dairy fat). Uncertainties are not quoted for these quantities. For parameters which are not as strongly coupled (such as average diameter and polydispersity), an iterative process of fixing and varying different variables in each fitting run is used to work towards the most reasonable parameters. Estimated uncertainties are quoted to within a 20% increase in χ_ν^2.

2.2. Instruments

Small angle neutron scattering (SANS) measurements were made on the NG3 instrument and ultra-small angle neutron scattering (USANS)

[1] On BT5 $\Delta q_z = 0.117$ Å^{-1} but the nominal $q < 10^{-4}$ Å^{-1}).

measurements were made on the BT5 instrument (Barker et al., 2005). Both are located at the NIST Center for Neutron Research in Gaithersburg, Maryland. Background from the main beam comes up rapidly on BT5 at the lowest q and the minimum reliable q for making measurements on these samples was 3×10^{-5} Å^{-1}. Measurements at high-q are limited by the very rapid drop off of the USANS signal. As the counting times get longer the measurement duration increases dramatically (17 min per point) and neutron background becomes more important (around 1.5 counts per min). Again 4×10^{-3} Å^{-1} is a typical upper limit to q.

The SANS measurements cover a range from 10^{-3} to 0.2 Å^{-1} but the high q intensities are used primarily for calculating incoherent scattering, rather than detailed fitting.

The particle size distributions of the emulsions were determined using light scattering with a Malvern Mastersizer 2000 (Malvern Instruments Ltd., UK) and the Hydro 2000 Small Volume Sample Dispersion Unit and Controller working at 1500 rpm (Malvern Instruments Ltd., UK). Water was the dispersant, hence the refractive index for the solvent was set at RI = 1.33. When skim milk was measured, RI = 1.38, while measuring whole milk the refractive index was set to RI = 1.46. Unfortunately, the Mastersizer instrument cannot handle two RIs simultaneously, hence the measurement for CMs in the case of whole milk might be skewed. The measurement and background time was 12 s with three measurements per aliquot separated by a 5 s delay. An obscuration of ≈16% was used. This was achieved by dispersing between 1 to 3 drops of each product in the dispersion unit that was filled with deionized water. Reported values are the averages obtained automatically by the software using three individual measurements. Measurements were performed at room temperature (≈22 °C).

2.3. Materials

Static light scattering measurements were made on commercial milk available at grocery stores in Guelph, Ontario in October 2018. They were whole, homogenized milk and skim milk manufactured under the brand names Beatrice, Neilson, and Lactantia in Canada. The samples used at NCNR came from skim milk [0–0.5 (w/w) % of milk fat] and whole milk (3.25% MF). They were products of Foodhold USA in Landover, Maryland, USA as common, food-grade milk. The contrast series samples were produced by mixing milk with a prepared water sample in a 1:1 volume ratio. The prepared water samples contained a mix of D_2O (heavy water) and distilled water (H_2O). Values quoted for D_2O concentration are appropriate for the sample as a whole, not the prepared water sample. This dilution procedure limited the D_2O content for the sample to a maximum of 50%, which was sufficient to reach the matching point for CMs and FGs. Standard NCNR titanium sample cells with quartz windows were used (Krzywon, 2018). The samples were 1.0 mm thick with a diameter of 19 mm. Samples were held at 20 °C in the sample changer.

3. Results and discussion

3.1. Static light scattering

As a first step static light scattering (SLS) measurements were performed on skim milk at room temperature followed by SLS measurements on whole milk. The basic model for this colloid is a polydisperse population of protein micelles. These micelles may be composed of several hundred to a few thousand casein protein molecules of various types. The CMs are hydrated and contain calcium phosphate. The reported voluminosity or ratio of micelle volume to protein mass is 4.4 cm^3/g (de Kruif et al., 2012). The nutritional information listed on the milk carton is 8 g protein per 240 mL. If 80% of these are insoluble caseins (Dalgleish & Corredig, 2012) then there are 27 mg of casein protein per mL and the volume fraction for the micelles is 0.12. The density of skim milk at room temperature is 1.033 g/mL (Goff, 2019),

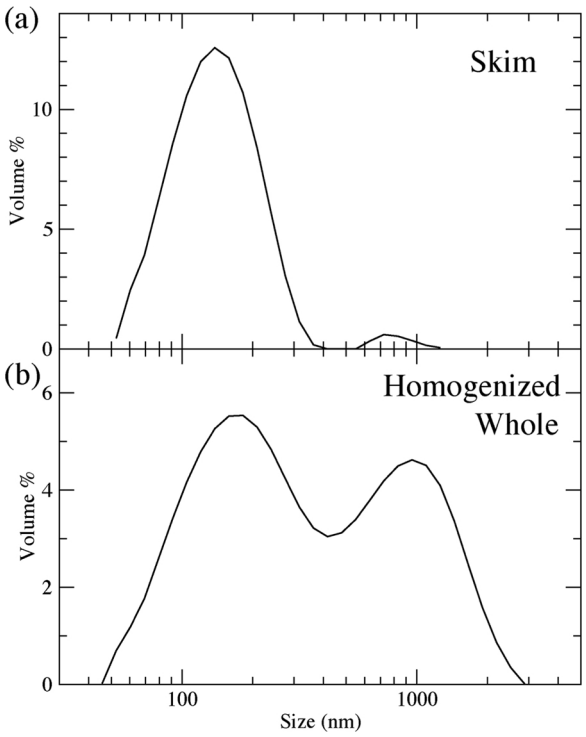

Fig. 1. Averaged static light scattering results from three commercial homogenized skim milks (a) and three homogenized whole milks (b). The peak to the left is interpreted to arise from the casein micelles while the peak to the right is interpreted as arising from the fat globules. The volume % values that are given on the y-axis are for scaling only, rather than absolute values.

which implies a mass fraction of 0.026. Although the protein mass ratio is seemingly low, the micelles do contribute to the optical opacity of skim milk. The basic single-population, polydisperse model for skim milk is consistent with the SLS measurements found in Fig. 1(a), which showed a single prominent population with a peak position at 140 nm, volume-weighted diameter $D_{4,3}$ = 148 nm and a surface-weighted diameter (Rawle, 2003) $D_{3,2}$ = 119 nm. The polydispersity is approximately 40% when the peak is fitted to a Schulz distribution. These results are the average of the three kinds of milk from Guelph, Canada. The signals from the different brands varied by less than 10%. The exact brand used for the neutron measurement was not included in the SLS measurement because the small variation seen in these three commercial brands provides some confidence that the structure is relatively consistent between brands.

Fig. 1(a) shows the SLS pattern for skim milk when a RI = 1.38 was used with a well defined peak centre around 100 nm. Fig. 1(b) shows the SLS pattern for whole milk. What was a small residual centred around 850 nm in skim milk (Fig. 1(a)) is now a peak comparable in size to the CM peak an centred at 950 nm. These peaks are interpreted as the signal from fat globules and, as expected from the homogenization process. The polydispersity resulting from a Schulz distribution fitted to the peak at 950 nm in Fig. 1(b) is 45%. When comparing the two data sets one can see a shift in the centre of the peak for CMs from 100 nm to 170 nm which may be due to a mismatch in index of refraction rather than a real change in the diameter of the CMs. For a weight percentage of fat 3.25% for whole milk, a density of milk fat of 0.915 g/cm^3 and a density of whole milk of 1.026 g/cm^3, the fat volume fraction can be calculated as 0.036 (Goff, 2019).

3.2. Neutron scattering of skim milk

With the particle size distribution of CMs and FGs in milk confirmed by SLS, neutron scattering was then employed to examine the milk

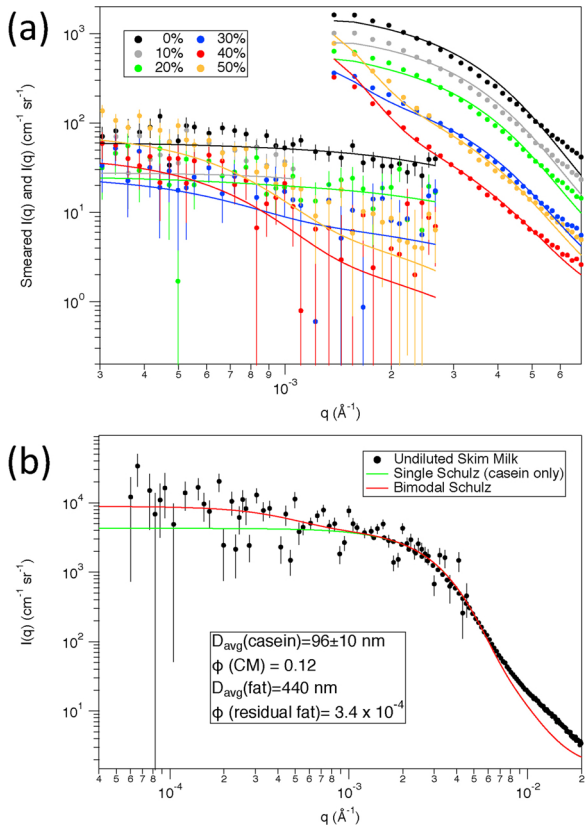

Fig. 2. (a) Global fits to a contrast series of diluted skim milk. The USANS data are to the left and are given as $I_s(q)$ while the SANS data to the right are given as $I(q)$. (b) Scattered intensity for skim milk as measured with SANS combined with desmeared USANS data. The red curve represents a model that includes residual fat while the green curve represents a model with no residual fat. (For interpretation of the references to colour in this figure legend, the reader is referred to the web version of this article.)

structure in more detail. One of the known problems is that the scattering signal from proteins is weak. There have been many SANS studies of skim milk that have concentrated on the CMs, and these have been reviewed by de Kruif (2014). Although steps could have been taken to enhance the CMs signal, such as using a sample from skim milk powder or evaporated milk to increase CM concentration, or using a serum based purely on D_2O where contrast could be increased, the goal of this particular measurement was not to discover new things about skim milk itself. Instead, the objective of the current study was to establish a baseline control-system of commercial milk that could be understood with neutron scattering over a wider range of q. This extension in range requires the inclusion of the signal from fat globules even in the residual concentrations present in skim milk.

In order to better study each system and their components, dilutions containing D_2O were used in both skim milk and whole milk. There is an extra complication for the CMs since, like other proteins or protein aggregates, the SLD of the CMs changes with D_2O concentration, unlike the FGs, which essentially stay at $\rho = 0.20 \times 10^{-6}$ Å^{-2} (Lopez-Rubio & Gilbert, 2009). Two key reasons for this dependence are the overall hydration of the micelle, where H_2O is replaced by D_2O, and proton/deuteron exchange between the protein and water (labile protons). Two methods are used to determine this variation in SLD. The first is to use global fitting results from the D_2O series to extract the SLD as a parameter. The second, model-independent method, is to use the scattering invariant Γ_0 after background signals have been removed.

3.2.1. Global fitting of the contrast series for skim milk

Fig. 2 is a summary of the neutron scattering measurements for the skim milk contrast series and the result for commercial skim milk with no modifications. As described earlier in Section 2.1.5, the data in Fig. 2 have had the scattering from the sample cell removed and have been converted to absolute units (cm^{-1} sr^{-1}), taking into account the transmission and the different counting times at the different q values. Fig. 2(a) includes both smeared USANS data and pinhole geometry SANS data on the same graph. As explained in Section 2.1.4 the data is not expected to overlap when presented in this form. This choice was made to avoid uncertainties using a numerical desmearing routine on the USANS data. The data were fit to a scattering model based on a bimodal Schulz distribution of spheres The model predicts $I(q)$ so Eq. (4) was used to produce an $I_s(q)$ to compare to the USANS. As expected for a global fit, several fitting and model parameters are kept at the same values for the different data sets (global variables). The concentration of CMs and FGs, their mean diameters and polydispersities, and the SLD of FGs are common to all of the model curves. The volume concentration of the CMs is held at 0.12, as explained in Section 3.1. The SLD of the FGs is fixed at $\rho = 0.20 \times 10^{-6}$ Å^{-2}. The SLD of the medium is fixed to a different value for each model curve. It is a simple linear function of fractional concentration x of D_2O that combines the SLD of the components prior to mixing.

$$\rho_{\text{medium}} = \frac{1}{2}(-0.48) + \frac{1}{2}[-0.56(1 - 2x) + 6.4(2x)] = -0.52 + 6.96x \tag{5}$$

SLD is in units of 10^{-6} Å^{-2} with x in volume fraction (rather than percentage) units. The value -0.48×10^{-6} Å^{-2}, that appears in Eq. (5) is the calculated SLD for the milk serum with no dilution. This is water including appropriate sugars and soluble whey protein. The factors of 2 and 1/2 account for the mixing procedure described in Section 2.3. The SLD of the CMs is left as a free parameter. Values for an incoherent flat background are found from the $I(q)$ beyond $q = 0.05$ Å^{-1} in the SANS data. This is different for each contrast measurement since H_2O and D_2O have different incoherent scattering lengths as well as different coherent scattering lengths.

As expected at the lower D_2O concentrations, a decreasing SLD difference between the medium and the majority CM component with x leads to a decrease in the overall signal up to the match point. This is made most clear by the SANS data on the right side of Fig. 2(a). After 40% D_2O concentration, the signal begins to increase again but with a slightly different shape near $q = 0.002$ Å^{-1}. The signal increase occurs because the match point has been crossed somewhere between 40% and 50% D_2O. The shape change is due to the increased contrast $(\Delta\rho)^2$ between the residual FGs phase and the medium, which has increased from 0.58×10^{-12} Å^{-4} to 7.6×10^{-12} Å^{-4}. The global fit, which includes this contrast factor, is able to account for this behaviour. As can

Table 1
Summary of results and parameters. These volume fractions were halved when fitting to milk mixed 1:1 with water. SLD are given in units of 10^{-6} Å^{-2}.

Phase	Parameter	Skim	Whole
CMs	Vol. Frac.	0.12[a]	0.12[a]
	Avg. D (nm)	96 ± 10	96[b]
	Polydispersity	0.33 ± 0.08	0.33[b]
	SLD (0% D_2O)	0.138 ± 0.014[c] −0.043 ± 0.010[d]	−0.043[b]
	SLD (50% D_2O)	2.83 ± 0.02[c,d]	2.8[b]
	Match point	43 ± 3 %	–
FGs	Vol. Frac.	$(3.4 \pm 0.8) \times 10^{-4}$	0.034 ± 0.002
	Avg. D (nm)	440 ± 100	470 ± 40
	Polydispersity	0.45[b]	0.45 ± 0.05
	SLD	0.20[a]	0.20[a]

[a] Parameter is fixed from a calculation or independent measurement.
[b] Taken from the results for the other sample.
[c] Calculated from the invariant.
[d] Calculated from a global fit.

be seen by the error bars and the data scatter, the signal in the USANS region from skim milk is small enough that it is comparable to the instrument sensitivity so it is not weighted as heavily as the SANS data in the global fitting procedure. This will not be the case for whole milk.

The model parameters and results from the global fit are given in Table 1 and the same results are used to generate the fits in Fig. 2(b). The overall fit quality is good and the agreement suggests that the CMs themselves are not strongly affected by whether or not measurements are made in milk rather than milk diluted with water (which has lower concentrations of the soluble milk components). It would also appear that micelle-micelle interactions are fairly small since this independent model works well and no change in fitting parameters is seen between a CMs volume fraction of 0.060 in Fig. 2(a) to 0.12 in Fig. 2(b). There are deviations at the higher q values where a simple model does not account for micelle substructure. For this reason the selected fitting region for SANS data is restricted to q below 0.007 $Å^{-1}$. The error bars on the USANS data are relatively large compared to the signal but overall, the intensity and shape are well described by the bimodal Schulz model within experimental uncertainties in the SANS and USANS regions.

The result for the average diameter of the CMs, 96 nm, is within the lower range of previously reported results from a variety of techniques. This value matches the SLS (Fig. 1) results that gave a size distribution in the range from 50 nm to 130 nm.

Results from fitting the data to the Schulz distribution showed that the polydispersity of the CMs is 0.33 (Fig. 2). This is in rough agreement with the width of the peak in Fig. 1. Polydispersity is difficult to determine as a free parameter using fitting techniques. It tends to couple into the average diameter and data that contain extra features at higher q give higher polydispersity parameters as an artifact of the fitting procedure. The result from Fig. 4 is used to set the polydispersity of the residual fat to be 0.45. Even when using contrast matching the small size of the residual scattering makes any other approach impractical.

Measurements of $I(q)$ for skim milk that include pinhole geometry SANS with USANS data that have been numerically desmeared are shown in Fig. 2(b). The displayed q range is somewhat larger than for the global fit since the single set is easier to see on the graph than multiple simultaneous data sets. One can see a discrepancy between the fit from the model and the data for $q > 0.007$ $Å^{-1}$. The numerical desmearing procedure allows for direct comparison of the two techniques and the data show excellent agreement in the overlap region of $q = 2 \times 10^{-3}$ to 4×10^{-3} $Å^{-1}$. The data agree with previously reported measurements in this q range (de Kruif, 2014). The solid red curve includes residual FGs and represents the best set of parameters to describe the data. The green curve has the same parameters except that the intensity of the fitted FGs signal has been set to zero to show the difference in signal from FGs.

The description of the data provided by both models in the intermediate q region is excellent. The red and green curves in Fig. 2(b) show the effect of residual fat in skim milk with no contrast matching. Due to large error bars in the USANS region the fit quality does not change dramatically, but even this small amount of fat changes the low q signal from roughly 4000 to 9000 cm s^{-1} sr^{-1}. As seen in the global fit the simple uniform spherical model performs less well at higher q values, which is to be expected since the accepted model of the CMs includes structure within the micelle (de Kruif, 2014). The low q data is fairly noisy but it would appear that the overall level of scattering is consistent with both the fat-free and residual fat model. The scattered intensity approaches $q = 0$ with a slope of zero. This fact alone establishes that the largest scattering objects in this sample are being observed and they do not form any larger structures over the accessible size range. Using $\phi = 0.12$, as determined earlier from the nutritional content and voluminosity of the CMs, the resulting SLD for a uniform CMs is -0.04×10^{-6} $Å^{-2}$. This value is much smaller than expected for a pure dairy casein protein (1.72×10^{-6} $Å^{-2}$), but is consistent with the model presented by de Kruif et al. (2012), which includes a significant amount of water and some calcium phosphate. The average

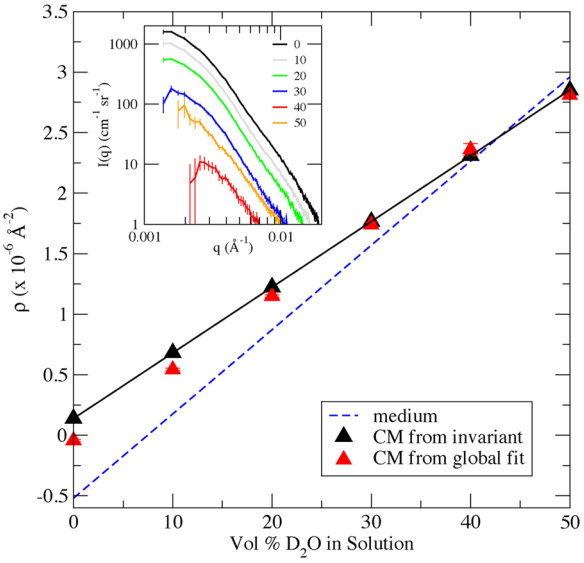

Fig. 3. Main: The SLD of the CMs resulting from invariant and global fit analysis as a function of D_2O concentration. For comparison sake the SLD of the medium from Eq. (5) is included as the dashed blue line. The straight line is a linear fit to the invariant results. Inset: $I(q)$ curves after the removal of incoherent background and a Porod form for residual fat.

diameter of D_{avg}(FGs) = 440 nm is slightly smaller than the result for homogenized milk (see Table 1). Comparing Fig. 1(a) and (b), one might want to conclude that the skimming process selectively removes the larger FGs, decreasing D_{avg}, and that this decrease persists even after homogenization of skim milk. The overall background signal arising from incoherent scattering is small and based on the measurements at higher q (not shown) the flat background is 1.54 cm $^{-1}$ sr^{-1}.

3.3. Determining the SLD of the casein micelles as function of heavy water content

The remaining result from the global fit is the SLD of the CMs and is shown in Fig. 3. As expected, it varies considerably with D_2O content but in a roughly linear manner. The match point is 43 ± 3 %.

The second method used to calculate the SLD of CMs is to calculate the invariant. The calculation in Eq. (2) should be performed on an $I(q)$ for a single phase in a medium. Looking at the integrand in Eq. (2) and the specific $I(q)$ it turns out that only a small fraction of Γ_0 comes from the USANS range. So rather than desmear the USANS data and include it in the invariant calculation, a Guinier model was used to extrapolate to low q. Unfortunately, despite the similarity of $I(q)$ for fat and fat-free models in Fig. 2(b), higher ρ_{medium} values that result from adding D_2O, enhance the residual FGs signal, while the CMs signal decreases. As seen in Fig. 2(a) the scattering curve not only changes in scale with $(\Delta\rho)^2$ (as expected), but also in shape, indicating either multiple phases, or a non-trivial interaction of D_2O with the sample, beyond a simple replacement. If the first case is assumed, and the FGs are the residual phase then it can be subtracted prior to the invariant calculation. In the SANS region a Porod model can be used to describe the fat signal to be subtracted from the data. In addition to the q^{-4} dependence, a scaling of the fat signal to $[\rho_{medium}(x) - \rho_{FGs}]^2$ needs to be included for each D_2O concentration.

$$I_{fat} \approx k(\rho_{medium} - 0.20 \times 10^{-6})^2 q^{-4} \quad (6)$$

where the approximation is appropriate for $q > 10^{-3}$ $Å^{-1}$ (the SANS region) and units for $I(q)$, ρ and q are as previously established. Choosing an overall proportionality constant of $k = 3.0 \times 10^{-10}$ and subtracting I_{fat} gives a set of corrected $I(q)$ curves for CMs only. This choice of k was the best value to maintain the shape with D_2O fraction

and best approach the $\Gamma_0 = 0$ or $\Delta\rho = 0$ match point. The implied amount of residual fat from this k is somewhat higher than expected based on the bimodal Schulz fits but still below 0.1% (w/w). These modified $I(q)$ curves are shown in the inset of Fig. 3. The solid black symbols represent the results of the invariant analysis after ρ_{CMs} is calculated using Eq. (3) with $\phi = 0.06$ for skim milk in a 1:1 volume ratio with water. The data closely follow an increasing linear trend $\rho = 0.138 + 5.43x$ (with the units and scales indicated on the figure and x as a fraction). Taking the intercept with Eq. (5) the match point is found at 43 ± 3 %, which agrees with the match point from the SLD results. However, the line does not match the SLD from the global fit at low values of D_2O concentration. These trends and results are in good agreement with the prediction of de Kruif et al. (2012) in their Fig. 1.

One explanation for the difference at low x between the methods is a change in curve shape because the single-phase invariant assumption is not true. The micelle does have separate water, protein and calcium phosphate components. The decrease in ρ at lower x for the fitting procedure compared to the invariant could result from a partition of total scattering strength between medium and high q that is different for D_2O and H_2O. Pure H_2O samples have more scattering at the higher q, representing a more pronounced inhomogeneity within the micelle. This is captured by the model-independent invariant but not by the q restricted global fit. D_2O concentrations up to the 50% limit reduce the inhomogeneities at short length scales and shift more of the signal to medium q. Such changes in scattering are at least consistent with a prominent shoulder at $q = 0.035$ Å^{-1} reported by several authors (de Kruif, 2014). A theoretical model and a scattering model to include structure within the micelle may help to explain this. A further test may be to use higher resolution small-angle X-ray scattering to investigate if D_2O would cause structural changes when added as a chemical/physical agent, rather than an inert contrast agent.

3.4. Using the bimodal Schulz model for whole milk

The next step was to add another phase to the colloid. The same model as that used for skim milk was employed, but the FGs were no longer a residual phase. FGs were the largest contributor to the USANS signal but gave a small SANS signal since the size of the FGs places it above the optimum size range for SANS. So contrast variation was used on a series of diluted whole milk samples with emphasis on USANS. The results are shown in Fig. 4 and both data and model are presented in smeared form. In principle, the 10% sample should be nearly contrast matched to fats. Since only the CM signal was expected, the shape should be similar to that for skim milk (as seen in Fig. 5 in smeared form). As observed with skim milk, the low-q signal has a zero slope (this is quite conclusive for 50% D_2O where the data scatter and uncertainties are quite small compared to the signal). This flat slope implies that the FGs are the largest structures accessible in this measurement range and are essentially independent (i.e., there is no aggregation). In the global model, volume fractions, average diameters, polydispersities and ρ_{FGs} are the same for every fit. The incoherent flat background was manually set for each concentration based on the high-q measurements for skim milk. The value of ρ_{medium} was based on Eq. (5) and the ρ_{CM} followed the red symbols of Fig. 3; the model independent SLD values from the invariant calculations could not account for the measured intensities at low D_2O concentrations. Considering that the individual parameters that determine intensities for each D_2O-series sample are globally fixed, the fits are quite good (overall reduced $\chi^2_\nu = 5.7$ for 321 observations) with good matches to low-q and medium-q intensities. As a test of the global fitting assumption, the parameters of SLD and size of the FGs were allowed to vary for each concentration on a separate basis. There was no appreciable improvement in fit quality over global variables. The results and model parameters are shown in Table 1.

The average diameter of FGs is slightly smaller than 0.5 µm. Again, this would be the D_{avg} based on diameter weighting rather than volume weighting. Polydispersity of the FGs seems larger than for the CMs but both values have significant uncertainties. Both are still roughly in agreement with Fig. 1. The FGs volume fraction is a free global variable and the result of 0.034 ± 0.002 is in excellent agreement with the prediction described in Section 3.1. The overall fit quality would also suggest that the CMs and FGs are independent of each other. Otherwise scattering might be observed from a shell or partial shell of CMs surrounding FGs, giving a length scale that matched FGs even when the FGs are rendered invisible by contrast matching. A model of CMs surrounding a FG as seen in micrographs would be useful to quantify this.

The global fits and contrast matching allowed for the separation of CM and FG signals in milk as seen in Fig. 5. There are no clear features in a single concentration USANS measurement (the solid black symbols) that can be used to conclusively distinguish the signals from the phases.

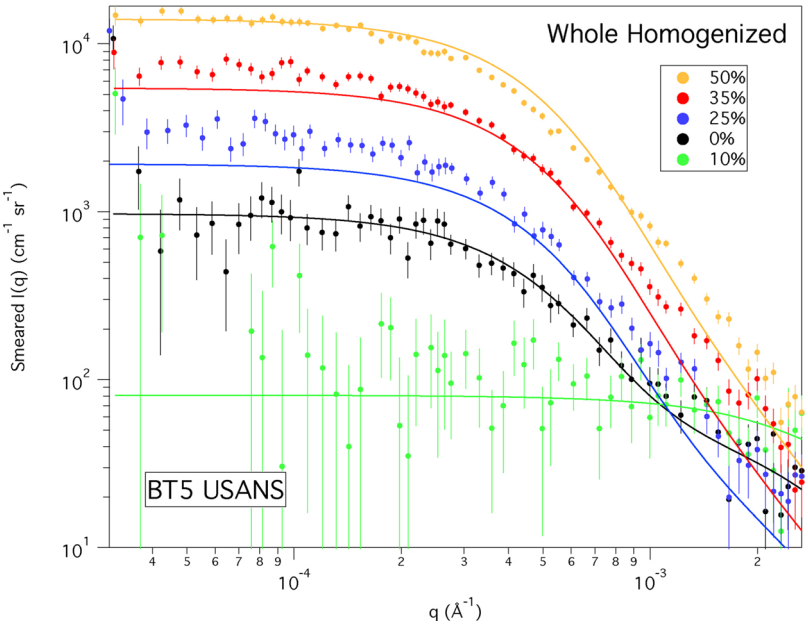

Fig. 4. USANS for measurements for the contrast matching series of whole milk as volume percentage of D_2O. The curves represent a global fit with the parameters in Table 1. The SLD of the medium is set by Eq. (5). The SLD of the CMs is based on the global fitting to the skim milk series.

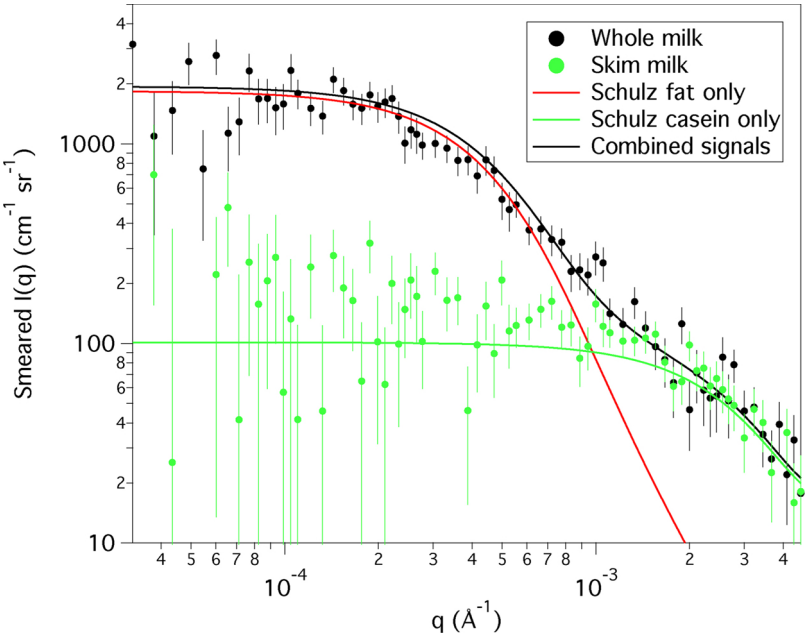

Fig. 5. USANS for undiluted commercial whole and skim milk with the scattering contributions from the different phases in the Schulz model.

Given the similarity of the CM portion of the model and the skim milk signal, subtracting skim from whole might have been a good starting point to isolate the fat signal, but contrast matching is much more conclusive. Without contrast matching the whole milk data, as is, would suggest a single empirical fit like Guinier–Porod (Hammounda, 2010) or a unified or Beaucage model (Beaucage, 1995, 1996), but this would definitely blur the two populations into one R_g and make extracting model parameters for SLD, volume fractions, etc. impossible. There is also some danger in using these empirical models over a relatively narrow range with only USANS since they fit data extremely well even when employed in a situation that is not matched to the appropriate physical model. It also would have been difficult to isolate the CMs signal without some SANS measurements to give information about the changing SLD.

The combined bimodal Schulz model (solid black line) in Fig. 5 gives an excellent overall description of the data ($\chi^2_\nu = 3.8$). The resulting ρ_{medium} (H_2O with some dissolved sugars and proteins) is -0.51×10^{-6} Å^{-2}, in agreement with the earlier prediction. The result ρ_{CM} (with no D_2O) is -3.7×10^{-11} Å^{-2}, or expressed with the usual scaling, $\approx 0.00 \times 10^{-6}$ Å^{-2}. This falls between the two results from the skim milk analysis in Fig. 3. Uncertainties for both of these are $\pm$ 0.02 $\times 10^{-6}$ Å^{-2}. All other parameters for Fig. 5 came from the global fits and match the values given in Table 1.

4. Conclusions

A combined SANS and USANS study of commercial homogenized skim and homogenized whole milk was carried out taking advantage of contrast variation. These measurements support a structural model based on polydisperse bimodal distribution of spheres that comprise casein micelles and fat globules. The parameters obtained are in agreement with previous measurements, using a variety of techniques, but this is one of the first times that fats and proteins have been combined in a sample for scattering measurements. As previously reported, there are some indications of curve shape changes or a non-trivial submicelle interaction with D_2O within the micelle. Extending measurements to the region where fats are prominent provides an excellent foundation for further structural measurements involving coagulated milk and cheese.

Declaration

Certain commercial equipment, instruments, or materials are identified in the text in order to adequately describe the experimental procedures. Such identification does not imply recommendation or endorsement by NIST.

Acknowledgements

This work was supported by the Natural Sciences and Engineering Research Council (NSERC) Discovery Grants program (CPA: Grant #249706-2012, AGM: Grant #05715-2015 and for DAP Grant #05362-2012), the St. Francis Xavier University Council for Research, and the Canada Research Chair Program. Access to BT5 was provided by the Center for High Resolution Neutron Scattering, a partnership between the National Institute of Standards and Technology and the National Science Foundation under Agreement No. DMR-1508249.

References

Alexander, M., Nieh, M.-P., Ferrer, M. A., & Corredig, M. (2011). Changes in the calcium cluster distribution of ultrafiltered and diafiltered fresh skim milk as observed by small angle neutron scattering. *Journal of Dairy Research, 78*(3), 349–356.

Barker, J. G., Glinka, C. J., Moyer, J. J., Kim, M. H., Drews, A. R., & Agamalian, M. (2005). Design and performance of a thermal-neutron double-crystal diffractometer for USANS at NIST. *Journal of Applied Crystallography, 38*, 1004–1011.

Beaucage, G. (1995). Approximations leading to a unified exponential/power-law approach to small-angle scattering. *Journal of Applied Crystallography, 28*, 717–728.

Beaucage, G. (1996). Small-angle scattering from polymeric mass fractals of arbitrary mass-fractal dimension. *Journal of Applied Crystallography, 29*, 134–146.

Bonse, U., & Hart, M. (1965). Tailless X-ray single-crystal reflection curves obtained by multiple reflection. *Applied Physics Letters, 7*, 238–240.

Dalgleish, D. G., & Corredig, M. (2012). The structure of the casein micelle of milk and its changes during processing. *The Annual Review of Food Science and Technology, 3*, 449–467.

de Kruif, C. G. (1999). Casein micelle interactions. *International Dairy Journal, 9*, 183–188.

de Kruif, C. G. (2014). The structure of casein micelles: A review of small-angle scattering data. *Journal of Applied Crystallography, 47*, 1479–1489.

de Kruif, C. G., Huppertz, T., Urban, V. S., & Petukhov, A. V. (2012). Casein micelles and their internal structure. *Advances in Colloid and Interface Science, 171–172*, 36–52.

Gebhardt, R., Doster, W., Friedrich, J., & Kulozik, U. (2006). Size distribution of pressure-decomposed casein micelles studied by dynamic light scattering and AFM. *European Biophysics Journal, 35*, 503–509.

Goff, P. H. D. (2019). *The dairy science and technology eBook, Dairy science and technology*

education series. Canada: University of Guelph. http://www.uoguelph.ca/foodscience/book-page/dairy-science-and-technology-ebook.
Grillo, I. (2008). Small-angle neutron scattering and applications in soft condensed matter. In R. Borsali, & R. Pecora (Eds.). *Soft-matter characterization* (pp. 723–782). Dordrecht: Springer.
Hammouda, B. (2010). *Probing nanoscale structure – The SANS toolbox.* Gaithersburg, MD: National Institute of Standards and Technology, NIST Center for Neutron Research. http://www.ncnr.nist.gov/staff/hammouda?the_SANS_toolbox.pdf.
Hammounda, B. (2010). A new Guinier–Porod model. *Journal of Applied Crystallography, 43*, 716–719.
Hansen, S., Bauer, R., Bredsted Lomholt, S., Bruun Quist, K., Skov Pedersen, J., & Mortensen, K. (1996). Structure of casein micelles studied by small-angle neutron scattering. *European Biophysics Journal, 24*(3).
Horne, D. S. (2006). Casein micelle structure: Models and muddles. *Current Opinion in Colloid & Interface Science, 11*, 148–153.
Ilavsky, J., Jemian, P. R., Allen, A. J., Zhang, F., Levin, L. E., & Long, G. G. (2009). Ultra-small-angle X-ray scattering at the advanced photon source. *Journal of Applied Crystallography, 42*, 469–479.
Jackson, A. J., & McGillivray, D. J. (2011). Protein aggregate structure under high pressure. *Chemical Communications, 47*, 487–489.
Kline, S. R. (2006). Reduction and analysis of SANS and USANS data using IGOR Pro. *Journal of Applied Crystallography, 39*, 895–900.
Kotlarchyk, M., & Chen, S.-H. (1983). Analysis of small angle neutron scattering spectra from polydisperse interacting colloids. *The Journal of Chemical Physics, 79*, 2461–2469.
Krzywon, J. (2018). *Demountable titanium cells.* www.nist.gov/nist-center-neutron-research/sample-environment/sans-sample-environment-and-equipment/demountable.
Kuo, W.-Y., Ilavsky, J., & Lee, Y. (2016). Structural characterization of solid lipoproteic colloid gels by ultra-small-angle X-ray scattering and the relation with sodium release. *Food Hydrocolloids, 56*, 325–333.
Li, Z., Yang, Z., Otter, D., Rehm, C., Li, N., Zhou, P., et al. (2018). Rheological and structural properties of coagulated milks reconstituted in D_2O: Comparison between rennet and a tamarillo enzyme (tamarillin). *Food Hydrocolloids, 79*, 170–178.
Lopez, C., Cauty, C., & Guyomarc'h, F. (2015). Organization of lipids in milks, infant milk formulas and various dairy products: Role of technological processes and potential impacts. *Dairy Science and Technology, 95*(6), 863–893.
Lopez, C., Madec, M.-N., & Jimenz-Flores, R. (2010). Lipid rafts in the bovine milk fat globule membrane revealed by the lateral segregation of phospholipids and heterogeneous distribution of glycoproteins. *Food Chemistry, 120*, 23–33.
Lopez-Rubio, A., & Gilbert, E. P. (2009). Neutron scattering: A natural tool for food science and technology research. *Trends in Food Science & Technology, 20*, 576–586.
McMahon, D. J., & Oommen, B. S. (2008). Supramolecular structure of the casein micelle. *Journal of Dairy Science, 91*, 1709–1721.
Ong, L., Dagastine, R. R., Kentish, S. E., & Gras, S. L. (2010). The effect of milk processing on the microstructure of the milk fat globule and rennet induced gel observed using confocal laser scanning microscopy. *Journal of Food Science, 75*, E135–E145.
Ong, L., Dagastine, R. R., Kentish, S. E., & Gras, S. L. (2011). Microstructure of milk gel and cheese curd observed using cryo scanning electron microscopy and confocal microscopy. *LWT – Food Science and Technology, 44*, 1291–1302.
Pederson, J. S. (1993). Resolution effects and analysis of small-angle neutron scattering data. *Le Journal de Physique IV, 3*(C8) C8-491–C8-498.
Rawle, A. (2003). The basic principles of particle size analysis. *Surface Coatings International Part A: Coatings Journal, 86*, 58–65.
ReportBuyer (2014). *Global dairy industry – The milky way*http://www.prnewswire.com/news-releases/global-dairy-industry—the-milky-way-271782401.html.
Roe, R.-J. (2000). *Methods of X-ray and neutron scattering in polymer science.* New York: Oxford Univ. Press.
Sears, V. F. (1992). Neutron scattering lengths and cross sections. *Neutron News,* 26–37.
Stothart, P. H. (1989). Subunit structure of casein micelles from small-angle neutron-scattering. *Journal of Molecular Biology, 208*(4), 635–638.
Stothart, P. H., & Cebula, D. J. (1982). Small-angle neutron scattering study of bovine casein micelles and sub-micelles. *Journal of Molecular Biology, 160*(2), 391–395.
Tromp, R. H., & Bouwman, W. G. (2007). A novel application of neutron scattering on dairy products. *Food Hydrocolloids, 21*, 154–158.
van Heijkamp, L. F., de Schepper, I. M., Strobl, M., Tromp, R. H., Heringa, J. R., & Bouwman, W. G. (2010). Milk gelation studied with small angle neutron scattering techniques and Monte Carlo simulations. *The Journal of Physical Chemistry A, 114*, 2412–2426.